Dalton Transactions

ROYAL SOCIETY OF CHEMISTRY

PAPER

View Article Online
View Journal | View Issue

Cite this: *Dalton Trans.*, 2025, **54**, 6195

Modulating the catalytic properties of decavanadate hybrids using a mixed counterion strategy for selective oxidation of thiophene-based sulfides and detoxification of mustard gas simulant†

Kousik Routh, Aranya Kar and Chullikkattil P. Pradeep *

Selective oxidation of sulfides to sulfoxides, especially thiophene-based sulfides, is a challenging task. Herein, we report a mixed counterion strategy in polyoxometalate (POM) chemistry to tune the selectivity of sulfoxidation reaction catalyzed by decavanadate cluster-based hybrids using H_2O_2 as the oxidant under ambient conditions. By employing two different aryl sulfonium counterions (ASCIs) bearing different organic functional groups (phenol/aldehyde/salicylaldehyde/2,6-diformyl phenol) in a 1 : 1 synthetic feed ratio, we have generated a series of decavanadate-based hybrids **HY1–HY6**. Different functional groups on the periphery of hybrids **HY1–HY6** helped control the efficiency and selectivity of the sulfoxidation reaction by fine-tuning the electronic and supramolecular effects of these hybrids as catalysts. Further, these hybrids were also applied as catalysts for detoxifying 2-chloroethyl ethyl sulfide (CEES), a mustard gas simulant. The hybrid **HY5**, with a structural formula $(DFHPDS)_2(FPDS)_2[H_2V_{10}O_{28}](H_2O)_3$ (DFHPDS = (3,5-diformyl-4-hydroxyphenyl)dimethylsulfonium, and FPDS = (4-formylphenyl)dimethylsulfonium) showed the best catalytic properties in the series, with up to 99% conversion and 85% and 99% selectivity towards sulfoxide in the case of dibenzothiophene (DBT) and CEES, respectively. This study's findings open new avenues for tuning the catalytic properties of POM-based hybrids toward selective organic transformation reactions by using a mixed counterion strategy.

Received 14th January 2025,
Accepted 17th March 2025

DOI: 10.1039/d5dt00102a

rsc.li/dalton

Introduction

Polyoxometalates (POMs) represent a large group of anionic metal-oxo nanoclusters, typically formed by early transition metals (Mo, W, V, Nb, and Ta) in their highest oxidation states.[1–3] The metal centers in POMs show reversible redox behavior, making them useful in catalysis,[4] sensing,[5] and biomedical applications.[6–8] The anionic charge of the POM clusters is balanced by positively charged counterions, commonly consisting of alkali and alkaline earth metal ions like Li^+, Na^+, K^+, and Cs^+. Besides these, several types of cationic organic moieties are also employed as counterions to charge-balance the POM clusters, leading to stable and robust Class I POM-hybrids. Choice and variation of the counterions can help fine-tune different interactions prevalent in POM-hybrids, including electrostatic, hydrogen bonding, van der Waals, and cation or anion-π interactions.[9] Studies have shown that the counterions can modulate a POM-hybrid's solubility, structure, and redox behaviors.[9] Therefore, in modern POM chemistry, the counterions are recognized as structural components that can control the overall properties of the cluster. Many reports have shown how the variation of counterions changes the catalytic,[10] biological,[11] self-assembly,[12] photo coloration,[13] and photocatalytic properties[14] of POM-based systems. Streb *et al.* showed that replacing a placeholder cation (dimethyl ammonium) of a POM cluster with a reactive metal cation allows tuning its redox properties, making it useful for multi-electron transfer and storage applications.[15] Further, Barteau *et al.* showed that increasing the countercations' concentration can modify the POM cluster's redox behavior.[16] These examples clearly show that the redox properties of a POM cluster may be tuned by altering the counterions, which in turn may affect its overall catalytic properties.

Polyoxovanadates (POVs) are an interesting sub-class of POMs consisting of vanadium metal centers. In recent years, researchers have shown increasing interest in the biological

School of Chemical Sciences, Indian Institute of Technology Mandi, Kamand – 175005, Himachal Pradesh, India. E-mail: pradeep@iitmandi.ac.in; Fax: +911905267 009; Tel: +91 1905 267 045

† Electronic supplementary information (ESI) available: Characterization data of all hybrids, details of catalytic oxidation of thiophene-based sulfide (PDF). CCDC 2346413. For ESI and crystallographic data in CIF or other electronic format see DOI: https://doi.org/10.1039/d5dt00102a

and catalytic activities of POVs due to their non-toxic nature and excellent redox properties.[17,18] Particularly, vanadium-containing POMs show superior activity as heterogeneous catalysts for sulfide oxidation reactions in the presence of H_2O_2.[19,20] Vanadium-based systems catalyze oxidation reactions in the presence of H_2O_2 by involving the V^{5+}/V^{4+} redox pair[21] and often their catalytic activity relies upon the efficient reversible conversion of this V^{5+}/V^{4+} pair.[21,22] Recent studies have also shown that the noncovalent interactions (NCIs) such as hydrogen bonding, C–H···π, C–H···F, C–H···O, C–H···Cl, C–H···H–C, lone pair···π, and π···π interactions play significant roles in catalytic processes.[23] Theoretical studies have shown that the NCIs between the different entities of the catalysis reaction, such as the catalyst and substrate,[24] ligands in the catalyst,[25] *etc*., can also play prominent roles in determining product selectivity.[26] In the POM-hybrids' case, the organic moieties or counterions associated with a POM cluster are crucial in controlling its overall redox property and noncovalent interactions with the substrates. This, in turn, can affect the overall catalytic efficiency and selectivity of POM-hybrid catalyzed reactions.[26]

Sulfide oxidation is an important organic transformation reaction critically connected with the oxidative desulfurization (ODS) of fuels, a successful strategy for removing sulfur components from fuel oils.[27] Thiophene-based sulfides in fossil fuels are harmful and must be removed for environmental reasons. However, in general, the thiophene-based sulfides are hard to oxidize. The oxidation of thiophene-based substrates often depends on the electron density of the sulfur; the higher the electron density of the sulfur, the more readily it can be removed by the oxidation process.[28] In general, the kinetics of sulfide oxidation reaction can be enhanced by using a catalyst at ambient temperature.[29] The oxidation of sulfide compounds in the presence of H_2O_2 and a catalyst can lead to the formation of different products, such as sulfoxides and sulfones. Most of the catalytic oxidation of sulfides reported in the literature results in complete substrate oxidation, generating sulfones. It is often difficult to control the selectivity of the reaction to yield the partially oxidized products, *i.e.*, sulfoxides, predominantly. At the same time, the synthesis of sulfoxides from sulfides has attracted much attention recently due to their utility for synthesizing biologically relevant molecules[30] and chiral molecules.[31] There have been several reports on polyoxovanadates (POVs)-based catalytic oxidation of sulfides,[32] but most of those studies have focused on the conversion of sulfides but not on the selectivity.[33–38]

The above discussions show that a POM hybrid's redox status and catalytic properties may be tuned by modulating the counterions. Further, the overall catalytic outcome of a reaction can be influenced by the noncovalent interactions between the catalyst and the substrate. In earlier work, we had shown that by employing organic counterions bearing salicylaldehyde-type functional groups, the catalytic activities of decavanadate-based hybrids could be controlled in the sulfide oxidation reaction.[13] This discovery opened up huge potential for tuning POM-hybrid-based catalysts for organic transformations using counterions bearing functional groups of different acidities, H-bonding properties, steric effects, *etc*. However, there were some practical difficulties associated with this approach. One such difficulty was the synthetic challenge in introducing multiple functional groups onto a single counterion moiety. This issue can be addressed using a mixed counterion strategy in which two or more different counterions bearing different functional groups are used in a POM hybrid. This approach will allow easy introduction of different organic functional groups onto a hybrid's periphery. The synergistic effects of these functional groups in controlling the redox and supramolecular properties of the POM-hybrid are expected to control their overall catalytic properties. However, there are only a few reports on POM hybrids where a mixed counterion strategy has been used to fine-tune their properties.[12,39,40] Therefore, there is plenty of scope in exploring this strategy for developing novel POM-hybrid-based materials and catalysts. In this work, we used different aryl sulfonium counterions (ASCIs) bearing different organic functional groups, such as aldehyde, phenol, salicylaldehyde and 2,6-diformylphenol, to develop mixed counterion POM hybrids so that multiple functional groups are introduced comparatively easily onto a POV cluster, $[H_2V_{10}O_{28}]^{4-}$ (decavanadate cluster). Accordingly, we synthesized mixed ASCIs based decavanadate hybrids having the formula $(FHPDS)_2(HPDS)_2[H_2V_{10}O_{28}]$ (**HY1**), $(FHPDS)_2(FPDS)_2[H_2V_{10}O_{28}]$ (**HY2**), $(HPDS)_2(FPDS)_2[H_2V_{10}O_{28}]$ (**HY3**), $(DFHPDS)_2(HPDS)_2[H_2V_{10}O_{28}]$ (**HY4**), $(DFHPDS)_2(FPDS)_2[H_2V_{10}O_{28}]$ (**HY5**), and $(DFHPDS)_2(FHPDS)_2[H_2V_{10}O_{28}]$ (**HY6**) (where FHPDS = (3-formyl-4-hydroxyphenyl)dimethylsulfonium; DFHPDS = (3,5-diformyl-4-hydroxyphenyl)dimethylsulfonium; FPDS = (4-formylphenyl)dimethylsulfonium and HPDS = (4-hydroxyphenyl)dimethylsulfonium), as shown in Scheme 1. The use of the ASCIs also helped to tune the overall solubility properties of the decavanadate cluster. The hybrids **HY1–HY6** were insoluble in ethanol, isopropyl alcohol and acetonitrile and were applied as heterogeneous catalysts for the sulfide oxidation reaction. These hybrids were also tested as catalysts for the oxidation of 2-chloroethyl ethyl sulfide (CEES), a simulant for the chemical warfare agent (CWA) bis-(2-chloroethyl)sulfide (mustard gas)[41] that causes severe skin damage, lung infection, eye irritation and even death at high concentrations.[42,43] Only a few reports in the literature exist on using POVs, especially decavanadate-based systems, as sulfide oxidation and mustard gas detoxification catalysts.[19,44–48]

Results and discussion

Synthesis and characterization

The aryl sulfonium counterion precursors, namely FHPDST ((3-formyl-4-hydroxyphenyl)-dimethylsulfonium triflate), HPDST ((4-hydroxyphenyl)-dimethylsulfonium triflate), FPDST ((4-formylphenyl)-dimethylsulfonium triflate) and DFHPDST ((3,5-diformyl-4-hydroxyphenyl)-dimethylsulfonium triflate) were synthesized following a reported procedure.[49] To synthesize the hybrids **HY1–HY6**, we followed a procedure reported for

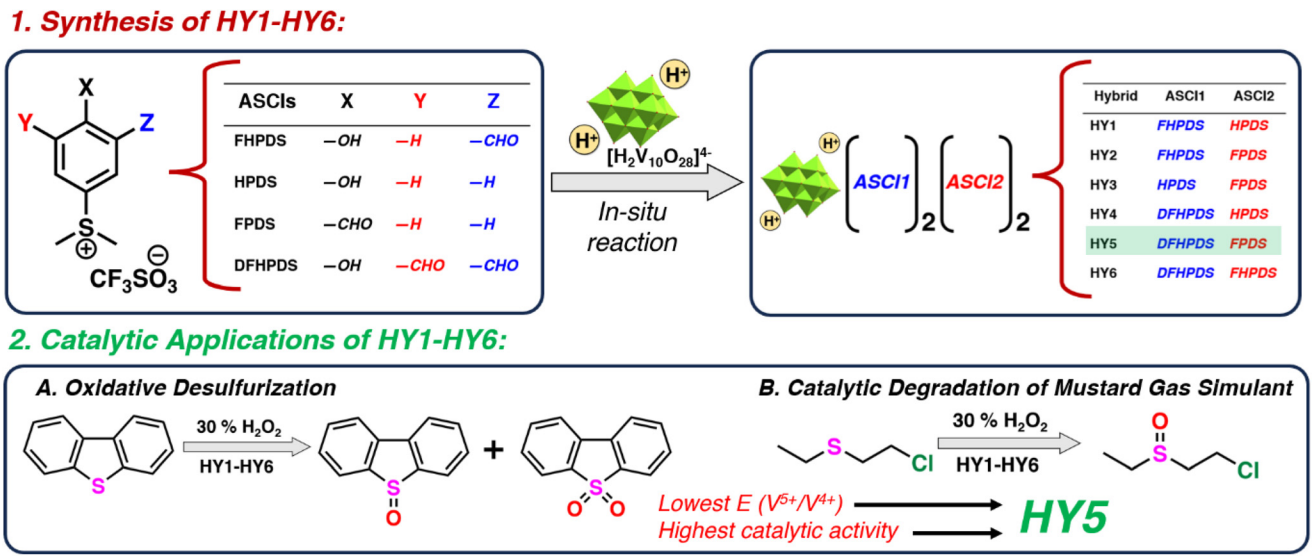

Scheme 1 Outline of the synthesis and applications of **HY1–HY6**.

similar materials.[11] In a typical reaction, for example, the synthesis of **HY1**, sodium metavanadate [$NaVO_3{\cdot}2H_2O$] (1 equivalent) was dissolved in water at elevated temperature (80 °C), then cooled down to room temperature and the pH was maintained at 4.5 with 4 M HCl to promote the formation of decavanadate anions in the solution. Parallely, a solution of 1 : 1 mixture of two different aryl sulfonium counterions precursors, *i.e.*, FHPDST and HPDST, was prepared in acetonitrile, which was then added dropwise into the decavanadate solution prepared above, resulting in immediate precipitation. The obtained precipitate was stirred overnight, filtered, and washed at least three times with ethanol (EtOH) and diethyl ether (Et_2O) and dried at 40 °C. This process led to the formation of the hybrid $(FHPDS)_2(HPDS)_2[H_2V_{10}O_{28}]$ (**HY1**). The other hybrids $(FHPDS)_2(FPDS)_2[H_2V_{10}O_{28}]$ (**HY2**), $(HPDS)_2(FPDS)_2[H_2V_{10}O_{28}]$ (**HY3**), $(DFHPDS)_2(HPDS)_2[H_2V_{10}O_{28}]$ (**HY4**), $(DFHPDS)_2(FPDS)_2[H_2V_{10}O_{28}]$ (**HY5**), and $(DFHPDS)_2(FHPDS)_2[H_2V_{10}O_{28}]$ (**HY6**) were also synthesized similarly by using a 1 : 1 mixture of the respective aryl sulfonium counterions precursors; see Scheme 1.

The formation of the mixed counterion hybrids **HY1–HY6** was confirmed through several analytical and spectroscopic techniques, including elemental, NMR, FT-IR, XPS, and ESI-MS analyses. Elemental analyses of the hybrids **HY1–HY6** indicated the presence of four organic counterions per decavanadate cluster in these hybrids. The details of the elemental analyses are given in the Experimental section. In the FT-IR spectra of **HY1–HY6**, characteristic stretching vibrations of the POM cluster, such as the stretching vibrations of the V–O bonds, $\nu_s(V–O_t)$ and $\nu_{as}(V–O_b–V)$, were observed in the range of 950–990 cm^{-1} and 840–740 cm^{-1}, respectively. Additionally, the presence of the organic counterions was confirmed by aromatic 'C=C' stretch (1400–1600 cm^{-1}) and aromatic 'C–H' stretch (2910–3100 cm^{-1}) peaks. Notably, **HY3** showed intense FT-IR peaks at around 1090 cm^{-1} and 1692 cm^{-1}. These peaks can be assigned to the ν(O–H) bending of the 'C–OH' functionality of HPDS counterion and the hydrogen-bonded formyl group (ν(C=O)) of FPDS counterion, respectively; see Fig. 1. Therefore, it was clear that **HY3** contains both the counterions, *i.e.*, FPDS and HPDS. Likewise, **HY2** showed a strong peak at 1702 cm^{-1}, indicating the presence of FPDS counterion with a formyl group, and another sharp peak at around 1680 cm^{-1} corresponding to the hydrogen-bonded formyl group of the FHPDS counterion.[50] The FT-IR data of other hybrids also confirmed the presence of decavanadate clusters and mixed counterions, the details of which are given in ESI.†

As the FT-IR analyses indicated the presence of mixed organic counterions with different functional groups in hybrids **HY1–HY6**, we performed NMR analyses to determine the ratio of different organic counterions present. These analyses showed that in hybrids **HY1–HY6**, the two different organic counterions are present in a more or less 1 : 1 ratio, which agrees with their synthetic feed ratio. The detailed NMR analyses of a representative hybrid, *i.e.*, **HY1**, are given here, and similar analyses for the remaining hybrids are given in ESI (Fig. S2–S6†). Hybrid **HY1** comprises the counterions FHPDS and HPDS along with the decavanadate cluster. The proton NMR spectrum of **HY1** exhibited two singlets at δ 3.12 and 3.18 ppm in a 1 : 1 ratio, and each singlet integrated into six protons. These peaks are attributed to the $-^{+}S(CH_3)_2$ protons of HPDS and FHPDS counterions. Further, it showed a singlet peak corresponding to one proton at δ 10.13 ppm, assignable to the aldehydic proton, and three singlet peaks corresponding to one proton each at δ 7.98, 7.85 and 6.85 ppm due to aromatic C–H protons.[11,13] The above peaks are assigned to the FHPDS counterion.[13] Further, **HY1** showed two doublets at around δ 7.88 and 7.02 ppm with two proton integrations each, assignable to the aromatic C–H protons of the HPDS counterion. As the integration ratio of $-^{+}S(CH_3)_2$ protons

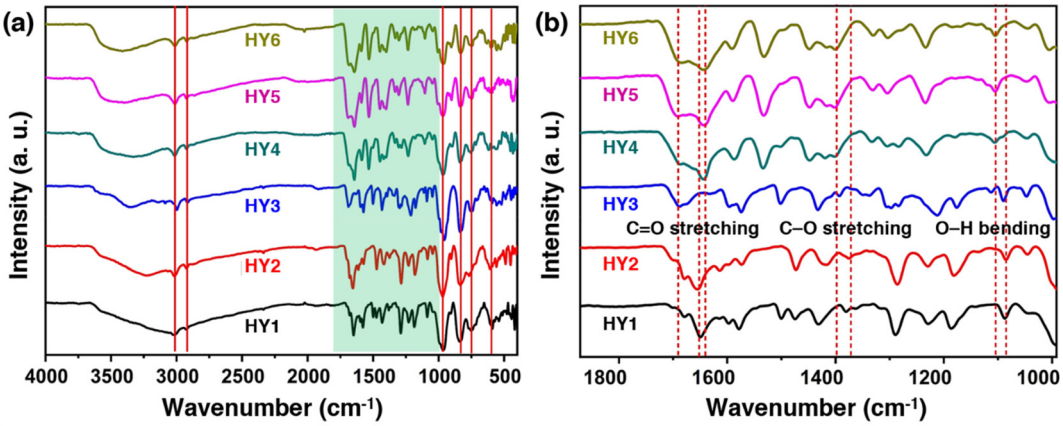

Fig. 1 (a) FT-IR spectra of **HY1–HY6**; and (b) zoomed-in view of the FT-IR spectra of **HY1–HY6** showing different stretching and bending modes of the counterions.

observed at δ 3.12 and 3.18 ppm was approximately 1 : 1 (HPDS : FHPDS), it suggests that the original feed ratio (1 : 1) of the counterions is maintained in hybrid **HY1**; see Fig. 2. Similarly, the detailed NMR analyses of the hybrids **HY2–HY6** also indicated the presence of two different organic counterions in a 1 : 1 ratio, matching the original synthetic feed ratio; see Fig. S2–S6, ESI.† Again, ^{51}V NMR spectra of **HY1–HY6** showed three peaks for three vanadium centers having different chemical environments. For example, the ^{51}V NMR spectrum of **HY1** exhibited three peaks at δ −418.67, −499.41, and −522.87 ppm, confirming the presence of a decavanadate cluster in the hybrid.[51] The detailed ^{51}V NMR analyses of the remaining hybrids are given in ESI (Fig. S7†).

The ESI-MS analyses of **HY1–HY6** were performed in the negative ion mode. The sample solutions for these analyses were prepared by dissolving minimum amounts of the hybrids in DMSO, followed by diluting with acetonitrile to a final concentration of approximately 10^{-6} M. Negative-ion ESI-MS analyses of **HY1**, **HY4**, and **HY6** revealed intense peaks at m/z 462.6262, 462.5788 and 462.5913 with 2^- charges, which are attributed to bare $[V_{10}O_{26}]^{2-}$ units. Similarly, **HY2**, **HY3**, and **HY5** exhibited intense peaks at m/z 462.6128, 462.7103, and

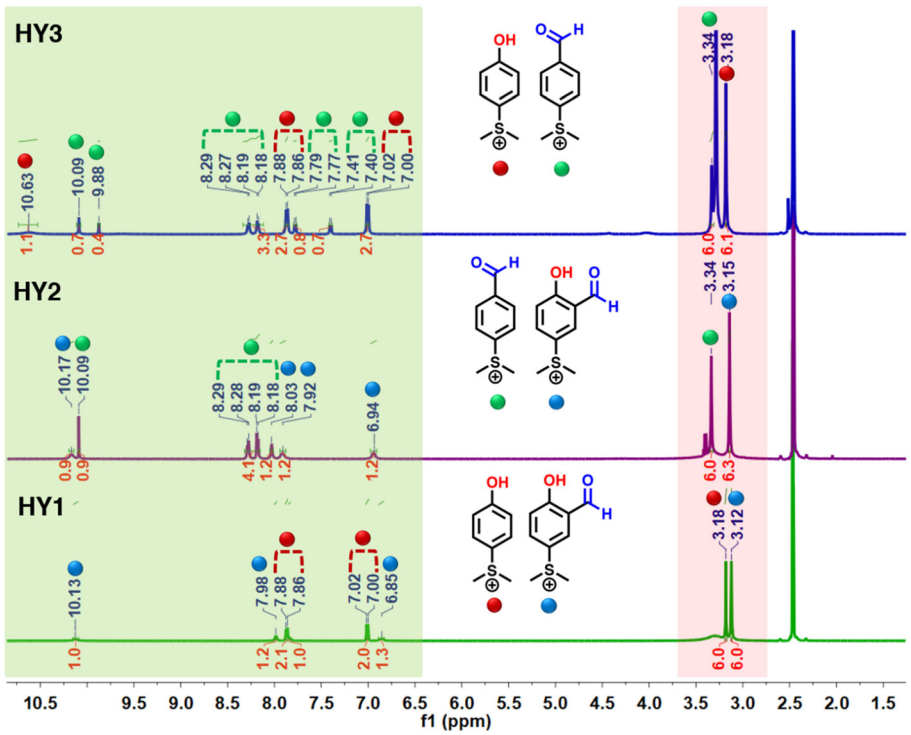

Fig. 2 ^{1}H NMR spectra of **HY1–HY3** in DMSO-D_6 solvent showing peak assignment due to different counterions.

462.6941 with 1^- charge corresponding to the half cluster moiety $[V_5O_{13}]^{1-}$. Interestingly, all the hybrids showed envelopes corresponding to the mixed counterion cluster species, confirming the formation of the mixed counterion POM hybrids as expected. For example, the ESI-MS data of hybrids **HY1–HY6** showed peaks at *m*/*z* 494.6133, 673.7867, 659.8673, 662.6035, 668.7777, and 676.7711 that are well matched to the mixed counterion species, $[V_{10}O_{28}(FHPDS)(HPDS)_2(H_2O)_2]^{3-}$, $[H_2V_{10}O_{28}(FHPDS)(FPDS)(H_2O)_2]^{2-}$, $[H_2V_{10}O_{28}(FPDS)(HPDS)(H_2O)_2]^{2-}$, $[H_2V_{10}O_{28}(DFHPDS)(HPDS)]^{2-}$, $[H_2V_{10}O_{28}(DFHPDS)(FPDS)]^{2-}$, and $[H_2V_{10}O_{28}(DFHPDS)(FHPDS)]^{2-}$, respectively. Therefore, the appearance of these peaks indicates the presence of mixed counterions in these hybrids. Detailed analyses of the negative-ion ESI-MS of the hybrids are given in Fig. S1–S6, ESI.† Further, the XPS analyses were conducted on **HY1–HY6** to confirm the presence of organic counterions and the decavanadate cluster. Carbon C 1s was used as an internal reference to calibrate the XPS spectra. The XPS survey of **HY1–HY6** showed peaks corresponding to vanadium, carbon, oxygen, and sulfur at their respective binding energies. Here, we have discussed the XPS data of only a representative hybrid, **HY5**, and the data of the rest of the hybrids are explained in Fig. S1–S6, ESI.† **HY5** contains two counterions: DFHPDS bearing 2,6-diformyl phenol functional groups and FPDS bearing '–CHO' functional group. To confirm the functional groups on the counterions in **HY5**, the carbon C 1s scan was deconvoluted. The C 1s peaks observed at 284.83, 285.49, and 286.25 were assigned to C═C/C–C, SP^3C, and C–O, respectively. At the same time, the C 1s peaks observed at 287.29 and 289.08 eV for **HY5** are due to the C═O groups on FPDS and DFHPDS.[13,52] The deconvoluted O 1s scan of **HY5** showed peaks at 531.5 and 532.7 eV due to the presence of 'C═O' (of DFHPDS and FPDS) and 'O–H' (of DFHPDS) functionalities confirming the presence of both the counterions. Further, the deconvoluted O 1s scan of **HY5** also showed peaks at 529.9 and 530.6 eV, corresponding to POM lattice oxygens.[52] The deconvoluted V 2p scan of **HY5** showed peaks at 517.29 eV and 524.70 eV, corresponding to V^{5+} $2p_{3/2}$ and V^{5+} $2p_{1/2}$, respectively. Similarly, the peaks observed at 516.06 eV and 523.17 eV are due to V^{4+} $2p_{3/2}$ and V^{4+} $2p_{1/2}$, respectively. Therefore, the XPS analyses revealed the presence of two different counterions along with the decavanadate cluster in the hybrids;[53] see Fig. 3.

Single-crystal X-ray diffraction analyses

The formation of the mixed counterion hybrids **HY1–HY6** was further confirmed by the single crystal X-ray analysis of a representative hybrid, **HY3**. The single crystals of **HY3** were grown from the mother liquor by a slow evaporation method. The crystallographic data of **HY3** are presented in Table S1, ESI.† **HY3** crystallized in the monoclinic $P2_1/c$ space group. The asymmetric unit consists of one-half of the decavanadate cluster and one unit each of the HPDS and FPDS counterions along with a water molecule, see Fig. 4. The aldehydic 'C═O' bond length of the FPDS counterion in **HY3** is 1.157 Å. The V–O bond distances in **HY3** agreed with the reported values for decavanadate-based hybrids.[19] The S–C bond distances and C–S–C bond angles of **HY3** are in the range of 1.773(5)–1.791(5) Å

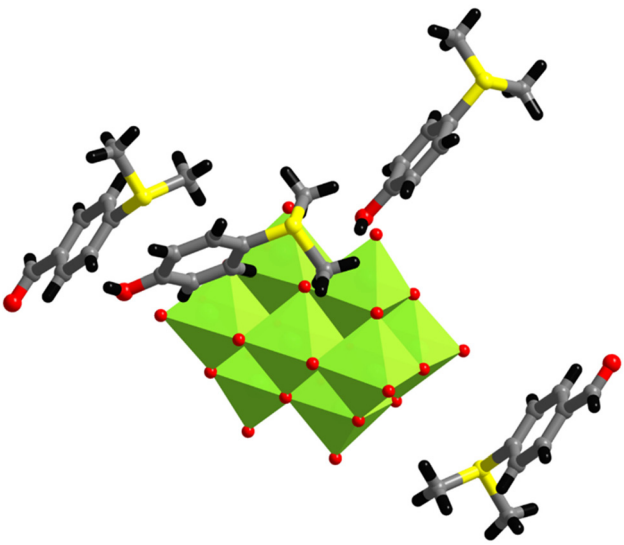

Fig. 4 Crystal structure of **HY3**. Color code: VO_6 – green octahedra; S – yellow; O – red; C – dark grey; H – black.

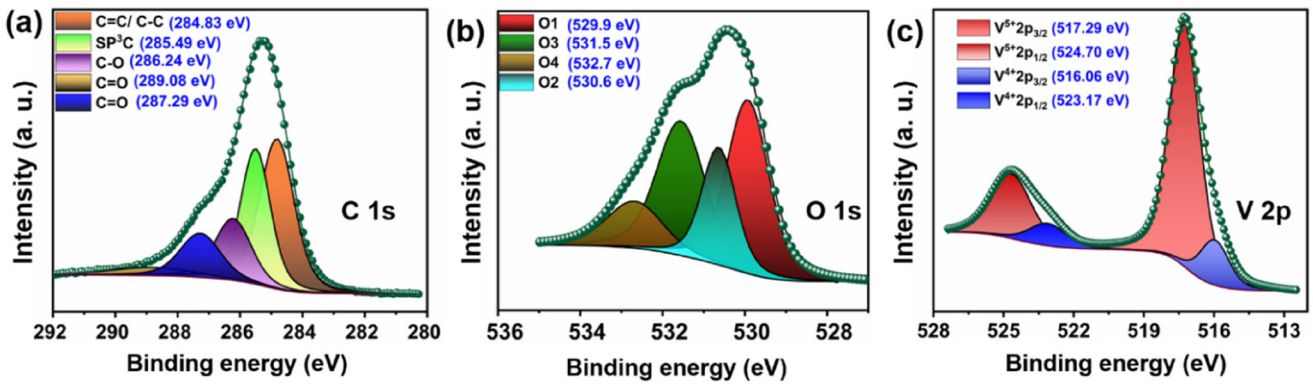

Fig. 3 Representative XPS spectra of **HY5** (a) C 1s; (b) O 1s; and (c) V 2p scans.

and 100.3(2)–105.30(19)°, respectively. As reported earlier, the C–S–C bond angles in **HY3** (less than 109°) confirm that the sulfonium centers adopt a trigonal pyramidal geometry.[54]

Our previous study has shown that the POM hybrids with mixed aryl sulfonium counterions bearing different functional groups can lead to intriguing self-assembled structures.[12] Therefore, we explored the morphological characteristics of **HY1–HY6** using Field Emission Scanning Electron Microscopy (FE-SEM), taking ethanol as the dispersion medium. The hybrids were dispersed in ethanol and drop cast over a silicon wafer, followed by solvent evaporation at 60 °C. The hybrids **HY1–HY6** showed different morphological features such as rods, spheres, sheets, *etc.*, indicating different self-assembly properties as a function of composition. The differences in the self-assembled structures of **HY1–HY6** indicate the existence of different interactions among the hybrids due to the presence of different functional groups on the counterions; see Fig. S10, ESI.† Further, we calculated the average particle sizes of **HY1–HY6** using FE-SEM image analyses. The calculated average particle sizes were ~373, 155, 448, 137, 197, and 130 nm, respectively, for **HY1–HY6**. These analyses show that the particle sizes of **HY4–HY6** are comparatively smaller than those of **HY1** and **HY3**, indicating larger surface areas; see Fig. S11, ESI.† Among **HY4–HY6**, **HY5** has a uniform particle size distribution and is uniformly dispersed.

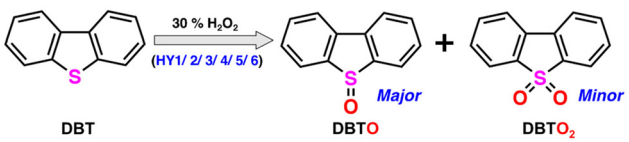

Scheme 2 Catalytic oxidation of DBT by using **HY1/2/3/4/5/6** as the catalyst.

Catalytic oxidation of sulfides

To check the catalytic abilities of **HY1–HY6** toward sulfide oxidation, we tested H_2O_2 mediated oxidation of dibenzothiophene (DBT) as a model reaction, as shown in Scheme 2. To optimize the reaction conditions, we first varied the experimental parameters, such as the catalyst dosage, reaction time, reaction temperature, and amount of oxidant. In each of these optimization reactions, **HY5** was used as the catalyst, and the reaction products were identified and confirmed by NMR and gas chromatography (GC) analysis; see Table 1. Three different reaction temperatures were tested, *i.e.*, 25 °C, 35 °C, and 45 °C, keeping the catalyst, substrate, and H_2O_2 amounts at 3 μmol, 0.246 mmol and 0.7 mmol, respectively. The results suggested that at 25 °C, the reaction proceeds only up to 71% in 2 hours under the above conditions. When the reaction temperature was increased to 35 °C and 45 °C (entries 3 and 4), the conversion reached 98% and 99% in 2 hours with 80% and 85% selectivity towards the sulfoxide derivative of DBT (*i.e.*, DBTO), respectively. However, raising the reaction temperature further up to 55 °C resulted in no further increase in the conversion, probably due to the decomposition of H_2O_2 at the higher temperatures.[55] Accordingly, the reaction temperature was optimized as 45 °C. We also checked the influence of factors like the dosage of the catalyst (entries 7 and 8) and solvent types such as acetonitrile, methanol, isopropyl alcohol (IPA) and dichloromethane (entries 11, 12, 13 and 14) on this catalytic reaction. Changes in the catalyst dosage did not yield encouraging results. Out of the solvents tested, ethanol, IPA and acetonitrile (ACN) exhibited good to moderate conversions of 99%, 92% and 90%, respectively, for oxidizing DBT. In addition to the best conversion, ethanol as solvent also led to good product selectivity (85%) towards sulfoxide compared to IPA (60%) and ACN (75%). Therefore, the optimized reaction conditions for the oxidation of DBT were finalized as 120 minutes of reaction time and ethanol as a solvent[56–58]

Table 1 Conversion and selectivity of the oxidation of DBT to DBTO in the presence of **HY5** with H_2O_2 as the oxidant in ethanol[a]

Entry	Catalyst (μmol)	H_2O_2 (mmol)	Time (h)	Temp. (°C)	Conv.[b] (%)	Selectivity[c] (%)
1	3	0.7	2	rt	71	40
2	3	0.7	4	rt	85	61
3	3	0.7	2	35	98	80
4	3	0.7	2	45	99	85
5	3	0.5	2	45	78	51
6	3	0.8	2	45	87	60
7	1.5	0.7	2	45	80	36
8	6	0.7	2	45	81	42
9	3	None	6	45	<1	<1
10	None	0.7	6	45	20	<5
11[d]	3	0.7	2	45	78	42
12[e]	3	0.7	2	45	90	75
13[f]	3	0.7	2	45	92	60
14[g]	3	0.7	2	45	10	<1
15[h]	3	None	24	45	<1	<1

[a] General reaction conditions (unless otherwise mentioned): ethanol as the solvent, 1.5 mL; substrate, 0.246 mmol; **HY5**, 3 μmol. [b] The conversion of DBT was confirmed by GC and NMR analysis. [c] Selectivity (towards sulfoxide) calculated using the formula, sulfoxide (mmol)/(sulfoxides (mmol) + sulfone (mmol)). [d] Methanol (1.5mL) as solvent. [e] Acetonitrile (1.5mL) as solvent. [f] 2-Propanol (1.5mL) as solvent. [g] Dichloromethane (1.5mL) as solvent. [h] Reaction condition: ethanol, 1.5 mL; substrate, 0.246 mmol; **HY5**, 3 μmol, O_2 balloon.

with the $n_{substrate} : n_{oxidant} : n_{catalyst}$ mole ratio of 1 : 3 : 0.012. Under these optimized reaction conditions, the hybrids **HY1–HY6** showed 10%, 79%, 75%, 94%, 99% and 98% conversion of DBT, respectively. Therefore, it can be noted that, among all the hybrids tested, hybrids **HY4–HY6** showed maximum conversion of DBT in less than 120 min. We also tested the DBT oxidation using molecular oxygen as an oxidant instead of H_2O_2 in ethanol. The results showed that the reaction did not proceed well even after 24 hours of reaction time, probably because the oxidation using molecular oxygen requires high pressure and temperature, see Table 1 (entry 15).[36,59,60] To explore the kinetics of the DBT oxidation reactions using **HY4–HY6** as catalysts, we calculated the reaction rate constants following the pseudo-first-order reaction kinetics; $\ln(C_0/C_t) = kt$ and $\ln k = -E_a/RT$, where C_0 and C_t correspond to initial DBT concentration and DBT concentration at different reaction times (t); k and E_a represent the rate constant and the activation energy, respectively. The $\ln(C_0/C_t)$ *vs.* reaction time plots are shown in Fig. 5(a–c), and the corresponding data are presented in Table S3, ESI.† The activation energies (E_a) for the reactions using **HY4–HY6** as the catalysts were calculated using the Arrhenius equation, which followed the order **HY4** (19.76 kJ mol^{-1}) < **HY5** (26.13 kJ mol^{-1}) < **HY6** (30.02 kJ mol^{-1}), see Fig. 5d. Also, we calculated the turnover frequency (TOF) of these reactions[29] to identify the best catalyst, which followed the order **HY5** (100 h^{-1}) > **HY6** (75.8 h^{-1}) > **HY4** (69.2 h^{-1}); Fig. S12, ESI.†

Several control experiments were also performed to fully understand the catalytic roles of **HY1–HY6** in the sulfide oxidation reaction. Firstly, the control experiments were performed using the counterion precursors of the hybrids, such as FPDST, HPDST, FHPDST, and DFHPDST, as the catalysts. Similarly, the decavanadate POM cluster having sodium counterions ($Na_6[V_{10}O_{28}]$) and a 1 : 1 mixture of the counterion precursors used to synthesize **HY5** (*i.e.*, DFHPDST & FPDST) were also tested as catalysts in separate control experiments. All the above control experiments showed only poor to medium catalytic efficiency (<1–48% conversion); see Table 2. The results of the control experiments show that the $Na_6[V_{10}O_{28}]$ cluster or the counterion precursors alone as catalysts are not adequate to give the high conversion, as observed in the case of **HY1–HY6** catalyzed reactions under the given conditions. These results, therefore, highlight the importance of the hybrids **HY1–HY6** in the observed catalysis.

The catalytic activities of **HY1–HY6** followed the order **HY5** > **HY6** > **HY4** > **HY2** > **HY3** > **HY1** in terms of percentage of conversion. Overall, **HY4–HY6** gave comparatively better catalytic conversion of DBT (*i.e.*, 94–99% conversion) than **HY1–HY3** (10–75% conversion). To get an idea about the better catalytic efficiencies shown by **HY4–HY6** compared to **HY1–HY3**,

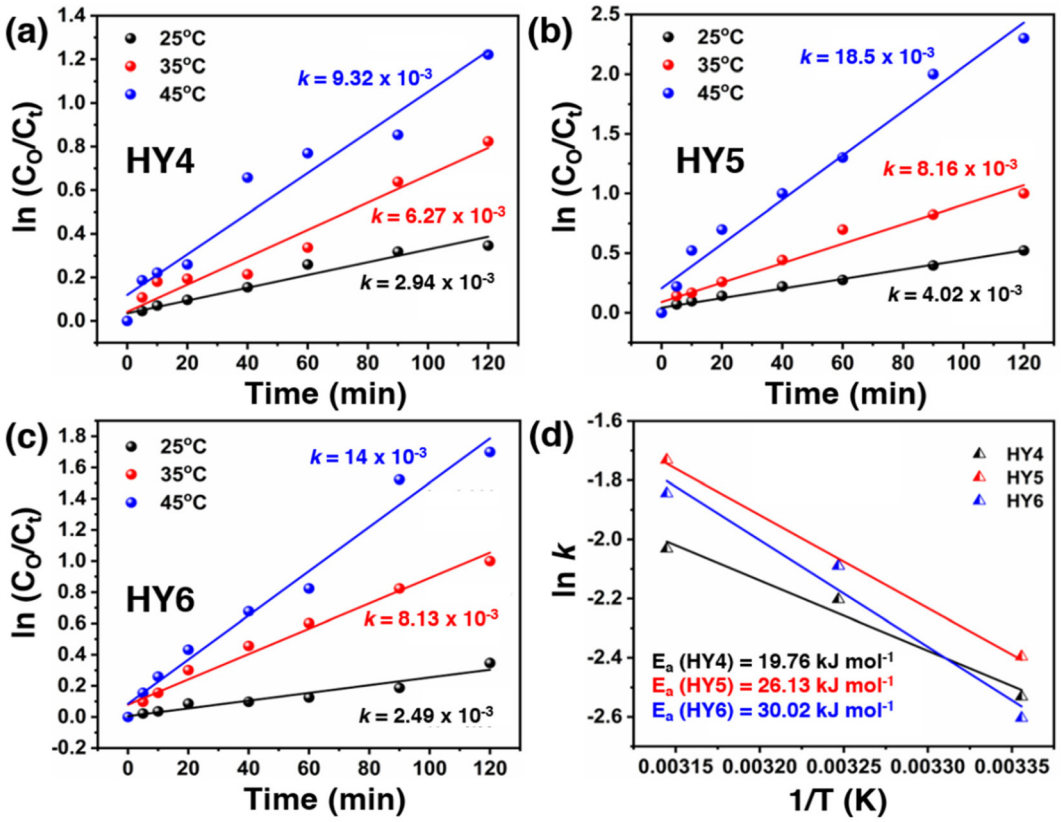

Fig. 5 (a), (b) and (c) Pseudo-first-order rate constant for DBT conversion at different temperatures using **HY4–HY6**; and (d) Arrhenius plots of **HY4–HY6**.

Table 2 Conversion and selectivity of the oxidation of DBT to sulfoxide using different catalysts with H_2O_2 as the oxidant in ethanol[a]

Entry	Catalyst	Conv.[b] (%)	Selectivity[c] (%)	System
1	**HY1**	10	<5	Heterogenous
2	**HY2**	79	29	Heterogenous
3	**HY3**	75	20	Heterogenous
4	**HY4**	94	55	Heterogenous
5	**HY5**	99	85	Heterogenous
6	**HY6**	98	60	Heterogenous
7	**1a**	99	81[d]	Heterogenous
8	**1b**	85	80	Heterogenous
9	$Na_6V_{10}O_{28}$	48	10	Heterogenous
10	$NaVO_3$	<15	<10	Heterogenous
11	DFHPDST	<1	<1	Homogeneous
12	FHPDST	<1	<1	Homogeneous
13	FPDST	<1	<1	Homogeneous
14	HPDST	<1	<1	Homogeneous
15	(DFHPDST : FPDST)	<1	<1	Homogeneous

[a] Reaction conditions: ethanol as the solvent, 1.5 mL; substrate, 0.246 mmol; catalyst, 3 μmol; temperature, 45 °C. [b] The conversion of DBT was confirmed by GC and NMR analysis. [c] Selectivity (towards sulfoxide, unless otherwise mentioned) calculated using the formula, sulfoxide (mmol)/(sulfoxides (mmol) + sulfone (mmol)). [d] Selectivity (towards sulfone) calculated using the formula, sulfone (mmol)/(sulfoxides (mmol) + sulfone (mmol)). **1a** ($(DFHPDS)_4[H_2V_{10}O_{28}]$)[13] and **1b** ($(FPDS)_4[H_2V_{10}O_{28}]$)[11] are previously reported decavanadate hybrids containing only a single type of aryl sulfonium counterions. These hybrids are used as control compounds to understand the roles of mixed counterions in the present study.

we used the Brunauer–Emmett–Teller (BET) method to calculate their surface areas using nitrogen adsorption–desorption isotherm (see Fig. S19, ESI†). The calculated surface areas varied for all the hybrids, where **HY4–HY6** showed significantly higher values of 79.95, 19.31, and 12.80 $m^2\ g^{-1}$, respectively, compared to **HY1** (6.32 $m^2\ g^{-1}$) and **HY3** (6.88 $m^2\ g^{-1}$). The only exception here was **HY2**, which had a calculated surface area of 15.43 $m^2\ g^{-1}$, similar to **HY5** and **HY6**, but exhibited comparatively poor catalytic activity. It is important to note here that while surface area can impact the activity of a catalyst, it is not always the case that a higher surface area leads to better catalytic efficiency. Several other structure–activity factors of the catalyst and substrate can also significantly determine the catalytic activity.[61] Again, to get a deeper insight into the better catalytic efficiency shown by **HY4–HY6**, XPS analyses were performed using V 2p scans of **HY1–HY6**. XPS data revealed that the percentage of V^{4+} in these hybrids followed the order **HY4** (24.1%) > **HY5** (23.7%) ≈ **HY6** (23.8%) > **HY3** (10.8%) > **HY2** (9.8%) > **HY1** (7.1%), see Fig. 6. These data revealed that the hybrids **HY4–HY6** possess a comparatively higher percentage of V^{4+} than **HY1–HY3**.

Cyclic voltammetry (CV) analyses of **HY1–HY6** were performed to determine their electrochemical properties in a heterogeneous medium; see Fig. S21(a) and (b), ESI.† All the electrochemical experiments were conducted using a three-electrode electrochemical cell, which employed a glassy carbon (GC) working electrode, Ag/AgCl (3 M) reference electrode, and a Pt wire counter electrode. **HY5** was used as a model compound to optimize the electrochemical conditions, *i.e.*, the pH and the purged gas (N_2/O_2). Firstly, the CV analysis of **HY5** was conducted by bubbling N_2 and O_2 gas separately in the electrolyte solution to investigate the influence of oxygen on the electrochemical properties of these materials, which are relevant in catalytic and oxidative environments. We found that in the presence of O_2, current density increases two times more than N_2, confirming that the presence of O_2 helps to regulate electron flow in the system; see Fig. 7(b). Interestingly, when we repeated the experiment with **HY1**, we observed no change in the current density, regardless of the presence or absence of O_2, see Fig. S20, ESI.† Based on the above observation, we can conclude that **HY5**, which has higher V^{4+} centers than **HY1** (as confirmed by XPS analyses), can produce more current in the presence of O_2. This is because O_2, as an oxidizing agent, can oxidize the reduced species present in the system, thus helping to regulate electron flow more effectively. Again, we optimized the pH under the O_2 atmosphere by using 0.1 M Na_2SO_4 as an electrolyte at two different pH conditions: (i) catalytic medium (pH = 3.5) and (ii) neutral (pH = 7). However, we did not use the basic condition as decavanadate is unstable under these conditions.[62] At pH 3.5, we observed more distinct peaks, corresponding to the V^{5+}/V^{4+} couple for three vanadium centers in the decavanadate cluster, compared to pH = 7, see Fig. 7(a). Therefore, we analyzed the CV of **HY1–HY6** in the scan range of +1.0 V to −0.8 V at pH 3.5 and in the presence of O_2. All the hybrids, **HY1–HY6** showed three quasi-reversible oxidation potentials at E = +0.23, 0.41 and 0.63 V, respectively, that may be attributed to the oxidation–reduction steps of vanadium.[63]

Again, differential pulse voltammetry (DPV) analyses of **HY1–HY6** were performed in an acidic 0.1 M Na_2SO_4 solution (pH 3.5) bubbled with O_2 to establish a connection between their catalytic activity and the oxidation potentials, see Fig. 7(c). The oxidation potential of V^{5+}/V^{4+} in **HY1–HY3** shifts to a higher oxidation potential in **HY4–HY6**. This indicates that the oxidation of V^{4+} in **HY4–HY6** is much easier than in **HY1–HY3**, increasing the likelihood of the formation of vanadium peroxo species and resulting in higher catalytic activity.

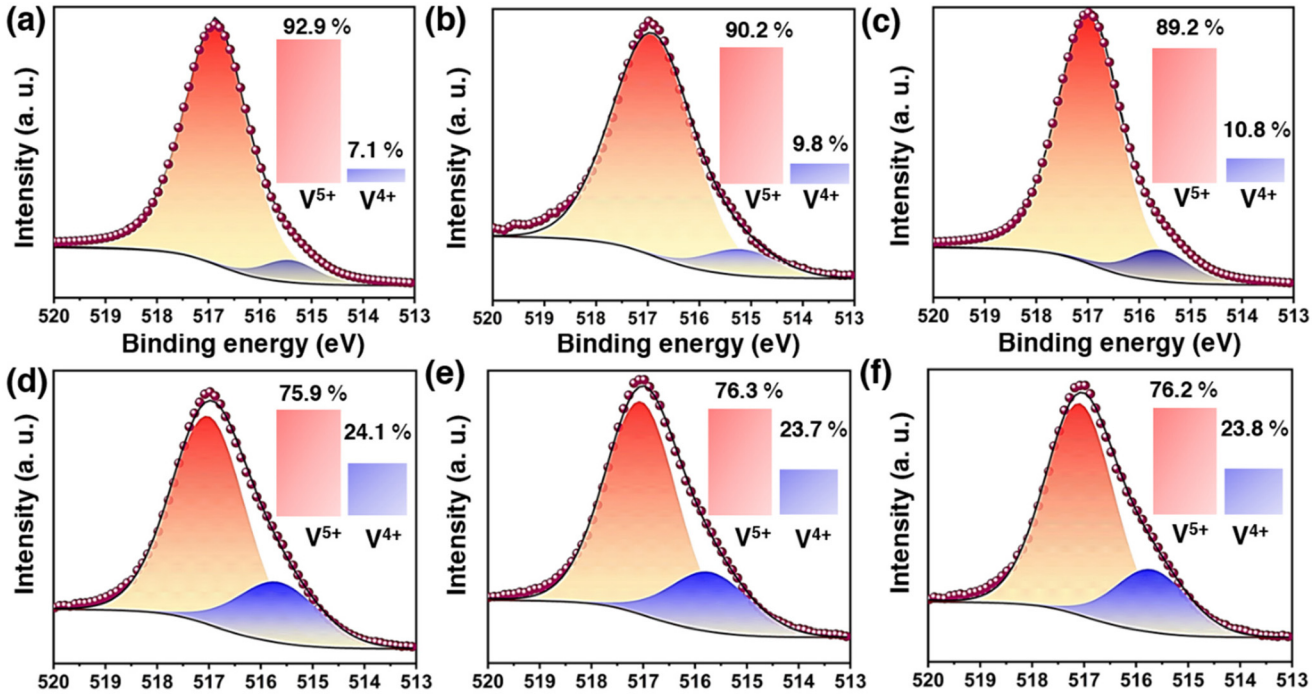

Fig. 6 Deconvoluted V 2p scans of (a) **HY1**; (b) **HY2**; (c) **HY3**; (d) **HY4**; (e) **HY5**; and (f) **HY6**.

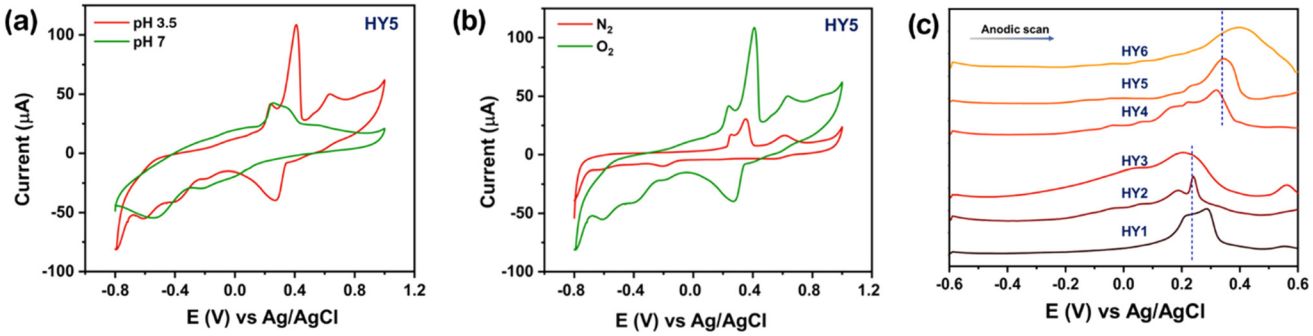

Fig. 7 Cyclic voltammograms (CVs) of (a) **HY5** in pH 3.5 and 7; (b) **HY5** in N_2 or O_2. Differential pulse voltammograms (DPVs) of **HY1–HY6** (c) anodic scan in 0.1 M Na_2SO_4 at pH 3.5. All the CVs were recorded at the scan rate of 50 mV s^{-1}.

Therefore, the XPS analyses showed a higher percentage of V^{4+} in **HY4–HY6** than in **HY1–HY3**, which is supported by the CV experiment. According to literature reports, often in vanadium-based catalytic oxidation reactions using H_2O_2, the vanadium (V^{4+}) gets oxidized by H_2O_2, forming vanadium peroxo-species that act as active catalysts for oxidation reactions.[64,65] This peroxovanadium then leads to the oxidation of sulfide/DBT and the peroxovanadium species is restored by reforming the catalyst for the next cycle, as previously reported, see Fig. S17, ESI.†[13] Therefore, in POV-based hybrids, forming the reversible redox pair V^{5+}/V^{4+} is one of the key factors for the reaction to proceed. Therefore, a greater % of V^{4+} species in the hybrid can contribute to a greater number of catalytically active sites for sulfide oxidation reactions. Further, the EPR analyses of the isolated **HY5** indicated the presence of some V^{4+}, showing eight-line EPR spectra with a g value of 2.01; see Fig. S23, ESI.† Depending on the interactions with the POM cluster, the counterions can modulate the redox potential of the cluster in the hybrid, which can further affect the V^{5+}/V^{4+} conversion and the catalysis rate.[66] Our earlier studies have shown that the DFHPDS counterions bearing a 2,6-diformyl phenol moiety can help in reducing the decavanadate cluster by providing acidic protons more readily.[13] Therefore, DFHPDS counterions in **HY4–HY6** could be a major factor behind their better catalytic properties compared to hybrids **HY1–HY3**, which do not contain any DFHPDS counterions. Among **HY4–HY6**, the percentage of V^{4+} in their composition was almost similar, and they showed almost similar conversion of DBT and the small variations in the catalytic activities among **HY4–HY6** could be due to the influence of the second counterions bearing different functional groups.

Based on the above discussions, we believe that several factors, such as the redox behaviors of the hybrid under catalytic conditions as indicated by the percentage of V^{4+} in XPS analyses, the particle size and dispersibility of the catalyst, the surface area of the catalyst, *etc*. could be playing roles in determining the catalytic trend shown by the hybrids **HY1–HY6** towards sulfide oxidation. However, more detailed theoretical and experimental analyses are required to fully understand the roles and reduction status of the catalyst in the catalytic oxidation reactions.

Selectivity of sulfide oxidation reaction

The oxidation of sulfides can lead to either sulfoxide or sulfone products, depending upon the reaction conditions. As mentioned earlier, sulfoxides are important precursors for synthesizing chiral[31] and biological compounds.[30] POVs can act as sustainable redox catalysts in oxidative desulfurization reactions by oxidizing thiophene-based sulfides, including DBT, DMDBT and BT, found in fuel oils. Several studies have reported using vanadium-containing POM-based catalytic systems to oxidize DBT. However, many of those studies are concerned only about the removal or conversion of the DBT, not the selectivity of conversion.[33,67,68] A few reports have focussed on conversion and selectivity, but most report selectivity toward the sulfone derivative.[13] On the contrary, the DBT oxidation data in Table 2 obtained using **HY1–HY6** as catalysts show selectivity toward sulfoxide products in general. **HY4–HY6** gave better selectivity towards sulfoxides (55–85%) than **HY1–HY3**, which gave a selectivity of (<5–29%) towards sulfoxides. Among all the hybrids, **HY5** gave the best catalytic activity regarding conversion (99%) and selectivity (85%) toward sulfoxide. Since the POM cluster (decavanadate cluster) is the same in all the hybrids and the experimental conditions employed were also the same, a major reason behind the observed differences in the catalytic selectivity could be the differences in the organic counterions and their effects in **HY1–HY6**. To check if the nature of the ASCs present in the hybrid catalyst has any role in determining the product selectivity of the sulfide oxidation reaction, we performed some additional control experiments as follows. As the hybrid **HY5** having the counterions DFHPDS and FPDS gave the best catalytic conversion and selectivity, we decided to perform control experiments using the hybrids having only one type of these counterions as catalysts. Accordingly, we synthesized two control compounds, $(DFHPDS)_4[H_2V_{10}O_{28}]$ (**1a**)[13] and $(FPDS)_4[H_2V_{10}O_{28}]$ (**1b**),[11] and tested their catalytic activities toward the oxidation of DBT under the optimized reaction conditions. These control experiments were conducted to understand if using mixed counterions (*i.e.*, a 1 : 1 combination of DFHPDS and FPDS in **HY5**) has any role in determining its catalytic properties. The results of these experiments suggested that when **1a** (having only DFHPDS counterions) was used as the catalyst, the product selectivity was toward sulfone (up to 81%) rather than sulfoxide. However, when **1b** (having only FPDS counterions) was used as the catalyst, the selectivity was toward sulfoxide (up to 80%). Therefore, under the experimental conditions, contradicting selectivities were obtained with hybrids with DFHPDS and FPDS counterions. Therefore, we can say that the nature of the aryl sulfonium counterions in **HY1–HY6** play significant roles in controlling their catalytic properties, especially the conversion and selectivity; see Table 2.

Various experimental parameters, such as the solvent system, oxidant amount and oxidant type, can affect the selectivity of oxidative desulfurization reactions.[56] It has also been shown that soft interactions, such as hydrogen bonding interaction between the catalyst and the substrate, play a match-winning role in stabilizing the catalyst's transition state, affecting the catalysis reaction's selectivity.[69] Besides, it is well accepted that the reversible redox potential of POM hybrids can be manipulated based on the soft interaction, such as intramolecular charge transfer between POM and the countercationic part, leading to selectivity in oxidative catalysis reaction.[22] The electronic and H-bonding effects of the functional groups on the aryl sulfonium counterions could play significant roles in determining the outcome of the reaction in the present case. **HY4–HY6** contains DFHPDS as one of the counterions, but the 2nd counterion varies in these hybrids. The organic functional groups on the 2nd counterion vary from a simple phenol to aldehyde to salicylaldehyde moieties. It may be noted that the presence of such different functional groups on the catalyst could influence the interactions between the catalyst and the substrate and control the outcome of the reaction. Recently, Suzuki *et al.* reported that the presence of methyl ethyl ketone (MEK) solvent bearing a C=O group in the reaction medium influences the catalytic outcome of sulfoxidation reaction using a POV-based hybrid as the catalyst.[70] Therefore, the different functional groups on the aryl sulfonium counterions in **HY1–HY6** could be playing different electronic and weak bonding interactions in the reaction media that affect their overall catalytic efficiency and selectivity. More detailed studies are, however, required to fully understand such an effect.

Considering the promising catalytic activity of **HY5** toward selective sulfide oxidation, we wanted to check its wider applicability as a catalyst using various thiophene and thioether-based substrates; see Table 3. Substrates with bulky substituents, such as diphenyl sulfide, were converted up to 98% with 70% selectivity towards sulfoxide (entry 1). In the present study, **HY5** was able to convert the thiophene-based sulfides, dibenzothiophene (up to 99% (entry 2)), benzothiophene (BT, up to 30% (entry 3)), and 4,6 dimethyl benzothiophene (up to 25% (entry 4)) to the corresponding sulfoxides. Here, BT has the least electron density on sulfur and showed a very low conversion rate. In the case of 4,6 dimethyl benzothiophene, the low conversion may be attributed to the steric effects of the two methyl groups besides the sulfur.[71] Overall, it is concluded that **HY5** can convert a variety of sulfides into their corresponding sulfoxides at 45 °C with impressive selectivity. Given this, the catalytic performance of **HY5** is quite different than the reported catalysts such as C_8V/g-BN,[46] $[C_8H_{17}N(CH_3)_3]H_3V_{10}O_{28}$,[72] which showed selectivity towards sulfone and

Table 3 Results of catalytic oxidation of different types of thiophene-based sulfides by **HY5** as a catalyst with 30% of H_2O_2 [a]

Entry	Substrate	Time (min)	Conversion[b] (%)	Selectivity[c] (%)
1	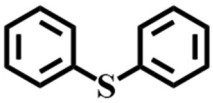	60	98	70[c]
2	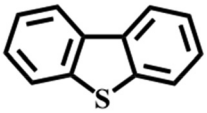	60	99	85[c]
3	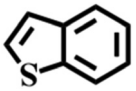	240	30	85[c]
4	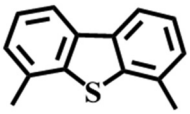	240	25	80[c]

[a] Reaction conditions: ethanol, 1.5 mL; substrate, 0.246 mmol; **HY5**, 3 μmol. [b] The conversion of DBT was confirmed by GC and NMR analysis. [c] Selectivity for sulfoxide = sulfoxide (mmol)/(sulfone (mmol) + sulfoxide (mmol)).

$[(C_2N_2H_8)_4(CH_3O)_4V^{IV}_4V^{V}_4O_{16}]\cdot 4CH_3OH$ (V_8-1),[73] which yielded sulfones and sulfoxides with less selectivity.

Stability and recyclability of the catalyst

The stability and recyclability of **HY1–HY6** as catalysts towards the oxidation of DBT were checked using a model catalyst, **HY5**, as it exhibited the highest catalytic activity among all the hybrids tested in this study. To confirm that the catalyst is stable under the reaction conditions and there is no leaching of vanadium, a thermal filtration experiment was performed in which the catalyst was filtered out from the reaction medium after 8 minutes, *i.e.*, after 60% conversion of the reactants, and the reaction was allowed to continue further. It can be seen from Fig. 8(a) that there is only a negligible amount of substrate conversion after the removal of the catalyst. This confirms that there is no considerable vanadium leaching into the reaction medium during the oxidation process. After five consecutive catalytic cycles, the percentage of DBT conversion decreased by less than 2% and selectivity decreased by only 5%, again showing that vanadium leaching is negligible in the present case. In general, some amount of metal leaching has been noted for POM-based catalysts in the literature during catalytic oxidation reactions.[68,69]

To check the recyclability of the catalyst **HY5**, it was recovered after five cycles of catalysis and subjected to ^{1}H NMR, FT-IR, ESI-MS, and XPS analyses. The ^{1}H NMR peaks of the recovered **HY5** (see Fig. S24, ESI†) matched that of the original **HY5**, suggesting no compositional change after catalysis. The FT-IR data showed that the stretching frequencies of the recovered catalyst match those of the fresh catalyst (Fig. S14, ESI†). Similarly, the ESI-MS data of the recovered catalyst in negative ion mode also showed the intactness of **HY5** after catalysis; see Fig. 8(b). Further, C 1s, O 1s and S 2p XPS scans of the recovered catalyst indicated there was no oxidation of the aldehyde functional group and the sulfonium center present in the counterion, discarding the possibility of any oxidation of the counterion moieties during catalysis. All these observations confirmed that the recovered catalyst remained stable; see

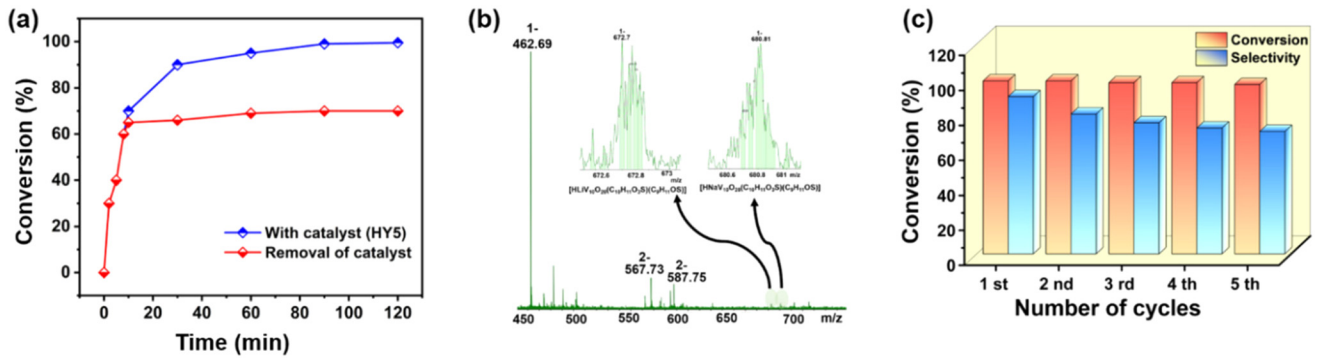

Fig. 8 (a) Catalytic dynamics (blue) and thermal filtration (red) of **HY5**; (b) ESI-MS analysis of the recovered catalyst; and (c) recyclability of catalyst (**HY5**) up to five cycles.

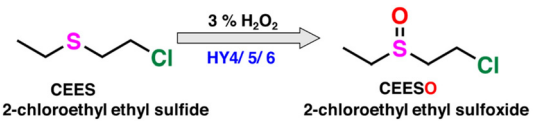

Scheme 3 Catalytic oxidation of CEES to CEESO using **HY4–6** as a catalyst.

Fig. S15, in ESI.† There was also no considerable decrease in the catalytic conversion after five cycles, which again proved the high recyclability of the catalyst.

Catalytic degradation of mustard gas simulant

Detoxification of hazardous chemical warfare agents (CWA) under mild conditions is extremely important in the current scenario of terrorist attacks and combats occurring in different parts of the world.[74,75] CWAs often cause damage to skin, lungs, eyes, and DNA. Considering the high toxicity and dangers of handling CWAs, experimentalists often use CWA simulants with similar structures and chemical behaviors for their studies. 2-Chloroethyl ethyl sulfide (CEES) is a promising and commonly used simulant for bis-(2-chloroethyl)sulfide (mustard gas or HD). Taking advantage of the better catalytic sulfide oxidation activity of **HY4–HY6**, we wanted to explore their potential to degrade CEES.[76–78] Most CWA detoxification studies using CEES simulant use O_2 (oxygen) as the oxidant, which requires a longer reaction time (~1 hour).[79] A lesser reaction time is possible with H_2O_2 as an oxidant, but it may also generate highly toxic sulfone as a side product along with the poorly toxic sulfoxide. Therefore, catalysts that can control the selectivity of CEES oxidation reaction towards sulfoxide in the presence of H_2O_2 is highly desirable.[80] **HY4–HY6** were tested for the catalytic oxidation of CEES by using 3% H_2O_2 (diluted with water) as the oxidant; see (Scheme 3). Here, we used 0.246 mmol CEES as the substrate, 1.5 mL of ethanol as the solvent and 0.492 mmol of 3% H_2O_2 as the oxidant at 25 °C. The progress of the reaction was monitored by gas chromatography and ^{1}H NMR analyses. Within 30 min of the reaction, hybrids **HY4**, **HY5** and **HY6** catalyzed the conversion of CEES to its sulfoxide in 81%, 99.5%, and 87% yields with turnover numbers (TON) of 66.42, 81.59 and 71.34, respectively. Among the hybrids tested, **HY5** gave the best catalytic activity. **HY5** catalyzed the conversion of CEES to its sulfoxide in 85% and 99.5% yields in 5 and 10 min of the reaction, respectively; see Fig. 9. Further, the reaction kinetics of the catalytic detoxification of CEES was investigated using **HY4–HY6** as catalysts under the optimized reaction conditions at 25 °C, and the conversion rates were calculated as a function of time. The $\ln(C_0/C_t)$ *vs.* time plot showed a linear correlation for all hybrids, indicating first-order kinetics. The first order rate constants k_1, k_2 and k_3 calculated for **HY4**, **HY5** and **HY6** are 0.021, 0.092 and 0.012 min^{-1}, respectively (Fig. S16, ESI†). Therefore, we can see that all these hybrid catalysts showed more or less similar catalytic behaviors, but **HY5** showed comparatively better activity in terms of the conversion rate.

Conclusions

A mixed counterion strategy used two different aryl sulfonium counterions (ASCIs) bearing different organic functional groups in a 1 : 1 synthetic feed ratio to generate a series of decavanadate cluster-based hybrids for the first time. The use of

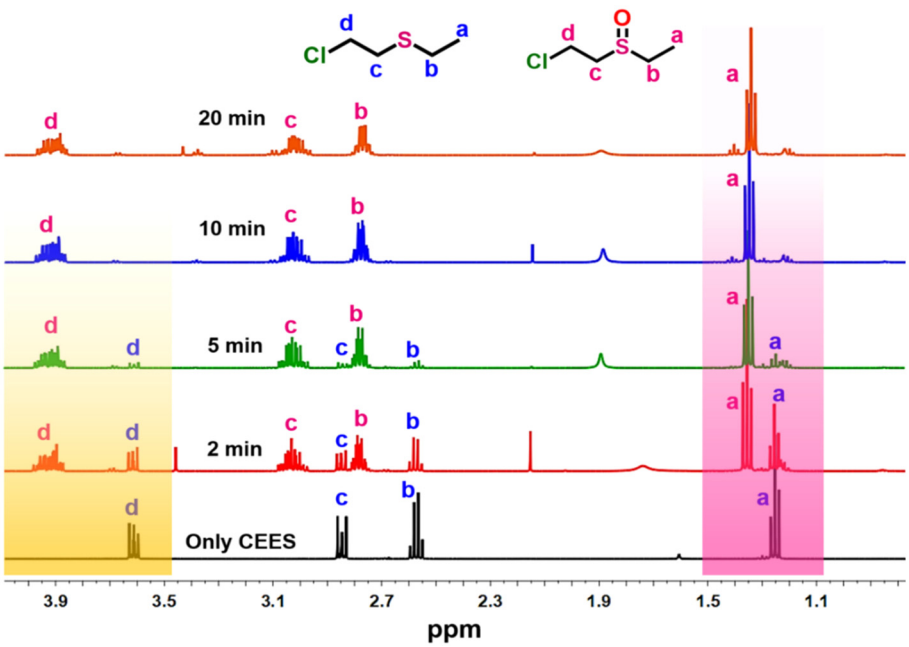

Fig. 9 Selected region of stacked ^{1}H NMR spectra of CEES, after 2, 5, 10 and 20 min of the reaction product by using $CDCl_3$ as a solvent.

different ASCIs allowed the facile introduction of different organic functional groups, such as phenol/aldehyde/salicylaldehyde/2,6-diformyl phenol, onto a POM hybrid. The use of mixed counterions bearing different functional groups has proven to be a powerful tool for controlling the supramolecular interactions and redox properties of the decavanadate hybrids, which in turn controlled their catalytic properties towards the selective oxidation of thiophene-based-sulfides to sulfoxides. In general, hybrids **HY4–HY6** having DFHPDS (ASCI with 2,6-diformyl phenol functional group) as one counterion showed better catalytic conversions than other hybrids. Hybrid **HY5** yielded 99% conversion and 85% selectivity towards sulfoxides in dibenzothiophene (DBT) oxidation. The ability of the counterions to control the V^{5+}/V^{4+} redox status and the supramolecular interactions of the cluster with the substrates played significant roles in controlling the catalytic conversion and selectivity in this study. Further, the organic counterions also helped to modulate the particle size and dispersibility of the catalysts, changing their surface area and affecting catalytic properties. In short, we have developed a series of mixed counterion incorporated decavanadate-based organic–inorganic hybrid materials exhibiting efficient catalytic properties towards the oxidation of thiophene-based sulfides and detoxification of mustard gas simulant. This strategy may be explored with different POM clusters and similar anionic clusters to generate a new series of selective catalysts for organic transformations. However, more detailed studies, including computational studies, are required to fully understand the selectivity switching observed here due to changes in the organic counterions of the hybrid catalysts.

Experimental section

Materials and method

Hexamethylenetetramine (HMTA) and trifluoro acetic acid (TFA) were purchased from Loba chemicals and Avra chemicals, respectively. 4-(Hydroxy) mercapto phenol, 4-(thiomethyl) benzaldehyde, dibenzothiophene 5,5′ dioxide, benzothiophene, and diphenyl sulfone were purchased from TCI chemicals. Dibenzothiophene, 4,6 dimethyl benzothiophene and silver trifluoromethane sulfonate were purchased from Sigma-Aldrich, and $NaVO_3{\cdot}2H_2O$ (sodium metavanadate) was purchased from Loba Chemicals. All the solvents used were of AR grade, and acetonitrile was distilled over CaH_2 before use.

Physical measurements

^1H, ^{13}C and ^{19}F NMR spectra were recorded on Jeol-JNM 500 MHz NMR spectrometer using $CDCl_3/D_2O$/DMSO-d_6 solvents and TMS as internal standard. FT-IR spectra were recorded on Agilent Technology Cary 600 series instrument. ESI-MS spectra were recorded on Bruker HD compact instrument. The X-Ray Photoelectron Spectroscopy (XPS) of the hybrids were recorded on a Thermo Scientific NEXSA photoemission spectrometer using Al-Kα (1486.6 eV) X-ray radiation. The raw data obtained from the instrument were processed using Avantage software. CHNS(O) elemental analysis was carried out in a Thermo Finnigan FLSH EA 1112 elemental analyzer. Inductively coupled plasma–mass spectrometry (ICP–MS) measurements were carried out using an Agilent 7850 LC-ICP-MS instrument after digesting the samples in concentrated nitric acid. Thermogravimetric analyses (TGA) were performed by using PerkinElmer Pyris 1 instrument. The sample (2 mg) was heated under a nitrogen atmosphere from room temperature to 800 °C at a heating rate of 10 °C min^{-1} with a flow rate of 20 mL min^{-1} in all of the TGA experiments. The X-ray powder diffraction data were recorded on a Rigaku SmartLab 9 kW rotating anode X-ray diffractometer in Bragg–Brentano configuration using a Cu-sealed tube (Cu-Kα X-rays of 0.1541 nm) operating at 45 kV and 100 mA. The measurements were taken in the 2θ range of 3–50° with a scan rate of 2° min^{-1} and a step size of 0.02°. The samples' morphological characterizations were performed using field emission scanning electron microscopy (FESEM, FEI Nova Nano SEM-450). Electron paramagnetic resonance (EPR) spectra were recorded at a temperature of 6 K using a Bruker ELEXSYS 580 EPR spectrometer.

Electrochemical measurements

Electrochemical experiments were conducted using a standard three-electrode cell. A catalyst-coated glassy carbon electrode (GCE) was used as the working electrode, Ag/AgCl (3 M) as the reference electrode, and Pt-wire as the counter electrode. The electrolytes used were 0.1 M H_2SO_4 aqueous solutions under an oxygen (O_2) atmosphere. To prepare the sample-modified electrodes, 4 mg of the compound, 1 mg of acetylene black carbon, and 20 μL of Nafion (aq) binder were mixed in 1 mL of isopropyl alcohol (IPA)/water mixture (4 : 1; v/v) and sonicated until a homogeneous suspension was formed. 20 μL of this mixture was coated onto the GCE using the drop-casting method, and the GCE was then dried under an IR lamp (temperature ~70 °C). All electrochemical experiments were conducted at ambient temperature.

X-ray crystallography

Single crystal X-ray diffraction data of **HY3** were collected on an Agilent SuperNova diffractometer equipped with multilayer optics, monochromatic dual source (Cu and Mo), and Eos CCD detector, using Mo Kα (0.71073 Å) radiation at 293 K. Data acquisition, reduction, and analytical face-index-based absorption correction were performed by using CrysAlisPRO program.[81] The structures were solved with ShelXS and refined on F^2 by full-matrix least-squares techniques using the ShelXL program provided in Olex^2 (v.1.2) program package.[81,82] Anisotropic displacement parameters were applied for all the atoms, except hydrogen atoms and some less intensely scattered carbon atoms. CCDC No: 2346413† contains supplementary crystallographic data.

Gas chromatography (GC) analyses

Gas chromatography analyses were performed on an Agilent 7890A series gas chromatograph equipped with an HP-5

column. A flame ionization detector (FID) and N_2 carrier gas were used for the sample analyses. Agilent open lab control panel software A.01.05 (1.3.19.115) was used to analyze the results and operate the GC system.

General procedure for the synthesis of HY1–HY6

The synthesis of a model hybrid, **HY1**, having the counterions FHPDS and HPDS, is described in detail here.

$NaVO_3{\cdot}2H_2O$ (0.5 g, 4.10 mmol) was dissolved in 20 mL of distilled water and heated to 80 °C for a clear, colourless solution. 4 M HCl was added dropwise to the reaction mixture to adjust the pH to 4.5. The color of the solution was changed to orange during this. Parallely, the counterion precursors FHPDST and HPDST were mixed in 1 : 1 molar ratio in acetonitrile to prepare a mixed counterion solution. This mixed counterion solution was then added dropwise into the decavanadate solution, leading to the formation of an instant yellow precipitate, which was stirred at room temperature for 12 h. After completion of the reaction, the reaction mixture was filtered and the precipitate obtained was washed with water (H_2O), ethanol (EtOH) and diethyl ether (Et_2O) several times and dried under vacuum at 40 °C to get a yellow-colored powder as the product.

Other hybrids **HY2–HY6** were also synthesized in a similar manner, using different counterion precursor mixtures FHPDST : FPDST/FPDST : HPDST/DFHPDST : HPDST/ DFHPDST : FPDST/DFHPDST : FHPDST, respectively. The control catalysts, **1a** and **1b**, were synthesized using the methods reported earlier.[11,13]

$(FHPDS)_2(HPDS)_2[H_2V_{10}O_{28}]$ (HY1). Yield: 30% based on V. Anal. calc. for **HY1**·H_2O: C, 24.68%; H, 2.92%; S, 7.75%; V, 30.79%; found: C, 24.31%; H, 2.7%; S, 7.32%; V, 31.19%. ^{1}H NMR (500 MHz, DMSO-d_6): $FHPDS^+$ cations, δ ppm 10.13 (s, 1H, Ar–CHO), 7.98 (s, 1H, Ar–H), 7.84 (s, 1H, Ar–H), 6.85 (s, 1H, Ar–H), 3.18 (s, 6H, –$S(CH_3)_2$); $HPDS^+$ cations, δ ppm 7.87 (d, 2H, J = 10 Hz, Ar–H), 7.01 (d, 2H, J = 10 Hz, Ar–H), 3.12 (s, 6H, –$S(CH_3)_2$). FT-IR (cm^{-1}): 3019 (w), 2923 (w), 1681 (sh), 1649 (sh), 1597(w), 1577(w), 1500(w), 1432 (w), 1228 (m), 1185 (m), 1087 (m), 1043 (m), ν (V═O, V–O–V), 963 (sh), 836 (sh), 750 (sh), 540 (m), 442 (w). ^{51}V NMR (105.2 MHz, DMSO-D_6): δ ppm −418.67, −499.41, −522.87.

$(FHPDS)_2(FPDS)_2[H_2V_{10}O_{28}]$ (HY2). Yield: 20% based on V. Anal. calc. for **HY2**·H_2O: C, 25.76%; H, 2.88%; S, 7.64%; V, 30.35%; found: C, 25.42%; H, 2.521%; S, 7.22%; V, 30.62%. ^{1}H NMR (500 MHz, DMSO-d_6): $FHPDS^+$ cations, δ ppm 10.17 (s, 1H, Ar–CHO), 8.03 (s, 1H, Ar–H), 7.92 (s, 1H, Ar–H), 6.94 (s, 1H, Ar–H), 3.15 (s, 6H, –$S(CH_3)_2$); $FPDS^+$ cations, δ ppm 10.09 (s, 1H, Ar–CHO), 8.27 (d, 2H, J = 10 Hz, Ar–H), 8.17 (d, 1H, J = 10 Hz, Ar–H), 3.34 (s, 6H, –$S(CH_3)_2$). FT-IR (cm^{-1}): 3012 (w), 2917 (w), 1702 (sh), 1680 (sh), 1654 (sh), 1595(w), 1572(w), 1474 (w), 1229 (m), 1182 (m), 1087 (m), 1043 (m), ν (V═O, V–O–V), 970 (sh), 833 (sh), 765 (sh), 535 (m), 450 (w). ^{51}V NMR (105.2 MHz, DMSO-D_6): δ ppm −412.43, −499.88, −524.23.

$(HPDS)_2(FPDS)_2[H_2V_{10}O_{28}]$ (HY3). Yield: 28% based on V. Anal. calc for **HY3**·H_2O: C, 25.17%; H, 2.98%; S, 7.91%; V, 31.40%; found: C, 24.85%; H, 2.79%; S, 7.51%; V, 31.68%. ^{1}H NMR (500 MHz, DMSO-d_6): $HPDS^+$ cations, δ ppm 10.63(s, 1H, Ar–OH), 7.88–7.86 (d, 2H, J = 10 Hz, Ar–H), 7.02–7.00 (d, 2H, J = 10 Hz), 3.18 (s, 6H, –$S(CH_3)_2$); $FPDS^+$ cations, δ ppm 10.09 (s) and 9.88 (s) (1H, Ar–CHO), 8.29–8.18 (dd, J = 10 Hz), 7.79–7.77 (d, J = 10 Hz), 7.41–7.40 (d, J = 5 Hz) (4H, Ar–H), 3.34 (s, 6H, –$S(CH_3)_2$). FT-IR (cm^{-1}): 3357(w), 3083 (w), 3000 (w), 2917 (w), 1692 (sh), 1670 (w), 1632 (w), 1594 (w), 1573 (w), 1431 (w), 1228 (m), 1175 (m), 1090 (m), 1043 (m), ν (V═O, V–O–V), 970 (sh), 833 (sh), 765 (sh), 557 (m), 445 (w). ^{51}V NMR (105.2 MHz, DMSO-D_6): δ ppm −421.46, −503.65, −521.40.

$(DFHPDS)_2(HPDS)_2[H_2V_{10}O_{28}]$ (HY4). Yield: 22% based on V. Anal. calc. for **HY4**·$3H_2O$: C, 24.76%; H, 3.0%; S, 7.34%; V, 29.17%; found: C, 24.23%; H, 3.15%; S, 6.89%; V, 29.63%. ^{1}H NMR (500 MHz, DMSO-d_6): $HPDS^+$ cations, δ ppm 10.71 (s, 1H, Ar–OH), 7.87 (d, 2H, J = 10 Hz, Ar–H), 7.01 (d, 2H, J = 10 Hz, Ar–H), 3.18 (s, 6H, –$S(CH_3)_2$); $DFHPDS^+$ cations, δ ppm 10.17 (s, 2H, Ar–CHO), 8.17 (s, 2H, Ar–H) 3.13 (s, 6H, –$S(CH_3)_2$). FT-IR (cm^{-1}): 3017 (w), 2921 (w), 1691 (w), 1639 (m), 1588 (w), 1531 (m), 1448 (w), 1231 (m), 1106 (w), 1090 (w), 1048 (w), ν (V═O, V–O–V), 963 (sh), 838 (sh), 750 (sh), 556 (m), 453 (w). ^{51}V NMR (105.2 MHz, DMSO-D_6): δ ppm −420.13, −502.31, −524.21.

$(DFHPDS)_2(FPDS)_2[H_2V_{10}O_{28}]$ (HY5). Yield: 28% based on V. Anal. calc. for **HY5**·$3H_2O$: C, 25.78%; H, 2.96%; S, 7.24%; V, 28.77%; found: C, 26.11%; H, 2.94%; S, 7.49%; V, 28.45%. ^{1}H NMR (500 MHz, DMSO-d_6): $FPDS^+$ cations, δ ppm 10.09 (s, 1H, Ar–CHO), 8.27 (d, 2H, J = 10 Hz, Ar–H), 8.17 (d, 2H, J = 10 Hz, Ar–H), 3.34 (s, 6H, –$S(CH_3)_2$); $DFHPDS^+$ cations, δ ppm 10.15 (s, 2H, Ar–CHO), 8.11 (s, 2H, Ar–H) 3.11 (s, 6H, –$S(CH_3)_2$). FT-IR (cm^{-1}): 3012 (w), 2926 (w), 1695 (w), 1643 (m), 1588 (w), 1531 (m), 1447 (w), 1234 (m), 1103 (w), 1046 (w), ν (V═O, V–O–V), 964 (sh), 838 (sh), 746 (sh), 575 (m), 459 (w). ^{51}V NMR (105.2 MHz, DMSO-D_6): δ ppm −420.24, −501, −522.84.

$(DFHPDS)_2(FHPDS)_2[H_2V_{10}O_{28}]$ (HY6). Yield: 31% based on V. Anal. calc. for **HY6**·$3H_2O$: C, 25.32%; H, 2.91%; S, 7.12%; V, 28.26%; found: C, 24.91%; H, 2.78%; S, 6.74%; V, 28.61%. ^{1}H NMR (500 MHz, DMSO-d_6): $DFHPDS^+$ cations, δ ppm 10.16 (s, 2H, Ar–CHO), 8.02 (s, 2H, Ar–H), 3.09 (s, 6H, –$S(CH_3)_2$); $FHPDS^+$ cations, δ ppm 10.16 (s, 1H, Ar–CHO), 8.23 (s, 1H, Ar–H), 8.13 (s, 1H, Ar–H), 7.22 (s, 1H, Ar–H), 3.21 (s, 6H, –$S(CH_3)_2$). FT-IR (cm^{-1}): 3007 (w), 2926 (w), 1687 (w), 1644 (m), 1590 (w), 1533 (m), 1448 (w), 1234 (m), 1102 (w), 1048 (w), ν (V═O, V–O–V), 963 (sh), 831 (sh), 746 (sh), 557 (m), 457 (w). ^{51}V NMR (105.2 MHz, DMSO-D_6): δ ppm −421.46, −500.57, −521.91.

Data availability

The data supporting this article have been included as part of the ESI.†

Conflicts of interest

The authors declare no conflict of interest.

Acknowledgements

C. P. P. thanks SERB, DST, Govt. of India for financial support (project no. CRG/2023/003151) and AMRC, IIT Mandi for infrastructural facilities. K. R. thanks the Council of Scientific and Industrial Research [CSIR SRF: 09/1058(0019)/2019-EMR-I] for a fellowship. K. R. thanks Suman Dolai for the assistance he provided in EPR experimental analysis. Rajesha Kumar Swain is sincerely thanked for his assistance in this study.

References

1 C. L. Hill, *J. Mol. Catal. A: Chem.*, 2007, **262**, 2–6.
2 D.-L. Long, R. Tsunashima and L. Cronin, *Angew. Chem., Int. Ed.*, 2010, **49**, 1736–1758.
3 H.-J. Lunk and H. Hartl, *ChemTexts*, 2021, **7**, 26.
4 N. Mizuno, K. Yamaguchi and K. Kamata, *Coord. Chem. Rev.*, 2005, **249**, 1944–1956.
5 P. Song and T. Wang, *ACS Sens.*, 2022, **7**, 3634–3643.
6 A. Bijelic, C. Molitor, S. G. Mauracher, R. Al-Oweini, U. Kortz and A. Rompel, *ChemBioChem*, 2015, **16**, 233.
7 A. Bijelic and A. Rompel, *Coord. Chem. Rev.*, 2015, **299**, 22.
8 A. Bijelic and A. Rompel, *Acc. Chem. Res.*, 2017, **50**, 1441–1448.
9 A. Misra, K. Kozma, C. Streb and M. Nyman, *Angew. Chem., Int. Ed.*, 2020, **59**, 596–612.
10 A. Kumar, A. K. Gupta, M. Devi, K. E. Gonsalves and C. P. Pradeep, *Inorg. Chem.*, 2017, **56**, 10325–10336.
11 K. Routh, S. Kaur and C. P. Pradeep, *Eur. J. Inorg. Chem.*, 2022, **2022**, e202200265.
12 A. Kar and C. P. Pradeep, *Inorg. Chem.*, 2022, **61**, 20561–20575.
13 K. Routh and C. P. Pradeep, *Inorg. Chem.*, 2023, **62**, 13775–13792.
14 M. Singh and C. P. Pradeep, *Dalton Trans.*, 2022, **51**, 3122–3136.
15 K. Kastner, J. Forster, H. Ida, G. N. Newton, H. Oshio and C. Streb, *Chem. – Eur. J.*, 2015, **21**, 7686–7689.
16 J.-J. J. Chen and M. A. Barteau, *Ind. Eng. Chem. Res.*, 2016, **55**, 9857–9864.
17 M. Aureliano, N. I. Gumerova, G. Sciortino, E. Garribba, C. C. McLauchlan, A. Rompel and D. C. Crans, *Coord. Chem. Rev.*, 2022, **454**, 214344.
18 M. Aureliano, N. I. Gumerova, G. Sciortino, E. Garribba, A. Rompel and D. C. Crans, *Coord. Chem. Rev.*, 2021, **447**, 214143.
19 X. Huang, X. Gu, Y. Qi, Y. Zhang, G. Shen, B. Yang, W. Duan, S. Gong, Z. Xue and Y. Chen, *Chin. J. Chem.*, 2021, **39**, 2495.
20 M. Sundararajan, B. Park and M.-H. Baik, *Inorg. Chem.*, 2019, **58**, 16250–16255.
21 J. Arichi, M. Eternot and B. Louis, *Catal. Today*, 2008, **138**, 117–122.
22 Y. Leng, J. Liu, P. Jiang and J. Wang, *Chem. Eng. J.*, 2014, **239**, 1–7.
23 Y. Reddi, C.-C. Tsai, C. M. Avila, F. D. Toste and R. B. Sunoj, *J. Am. Chem. Soc.*, 2019, **141**, 998–1009.
24 S. Ghosh, A. Changotra, D. A. Petrone, M. Isomura, E. M. Carreira and R. B. Sunoj, *J. Am. Chem. Soc.*, 2023, **145**, 2884–2900.
25 Y. Dangat, S. Popli and R. B. Sunoj, *J. Am. Chem. Soc.*, 2020, **142**, 17079–17092.
26 B. Chen, X. Huang, B. Wang, Z. Lin, J. Hu, Y. Chi and C. Hu, *Chem. – Eur. J.*, 2013, **19**, 4408–4413.
27 F. S. Mjalli, O. U. Ahmed, T. Al-Wahaibi, Y. Al-Wahaibi and I. M. AlNashef, *Rev. Chem. Eng.*, 2014, **30**, 337–378.
28 A. Rajendran, T.-y. Cui, H.-x. Fan, Z.-f. Yang, J. Feng and W.-y. Li, *J. Mater. Chem. A*, 2020, **8**, 2246–2285.
29 G. Ye, L. Hu, Y. Gu, C. Lancelot, A. Rives, C. Lamonier, N. Nuns, M. Marinova, W. Xu and Y. Sun, *J. Mater. Chem. A*, 2020, **8**, 19396–19404.
30 M. C. Carreno, *Chem. Rev.*, 1995, **95**, 1717–1760.
31 I. Fernández and N. Khiar, *Chem. Rev.*, 2003, **103**, 3651–3706.
32 B. Bertleff, J. Claußnitzer, W. Korth, P. Wasserscheid, A. Jess and J. Albert, *ACS Sustainable Chem. Eng.*, 2017, **5**, 4110–4118.
33 H.-M. Gan, C. Qin, L. Zhao, C. Sun, X.-L. Wang and Z.-M. Su, *Cryst. Growth Des.*, 2021, **21**, 1028–1034.
34 Y.-Q. Zhao, Y.-Y. Liu and J.-F. Ma, *Cryst. Growth Des.*, 2021, **21**, 1019–1027.
35 B. Bertleff, J. Claußnitzer, W. Korth, P. Wasserscheid, A. Jess and J. Albert, *Energy Fuels*, 2018, **32**, 8683–8688.
36 M. Okamoto, M. Watanabe and T. Yamaji, *J. Organomet. Chem.*, 2002, **664**, 59–65.
37 C. Komintarachat and W. Trakarnpruk, *Ind. Eng. Chem. Res.*, 2006, **45**, 1853–1856.
38 M. J. Poller, S. Bönisch, B. Bertleff, J. C. Raabe, A. Görling and J. Albert, *Chem. Eng. Sci.*, 2022, **264**, 118143.
39 V. Coué, R. Dessapt, M. Bujoli-Doeuff, M. Evain and S. Jobic, *Inorg. Chem.*, 2007, **46**, 2824.
40 R. Dessapt, M. Collet, V. Coué, M. Bujoli-Doeuff, S. Jobic, C. Lee and M.-H. Whangbo, *Inorg. Chem.*, 2009, **48**, 574–580.
41 L. Szinicz, History of Chemical and Biological Warfare Agents, *Toxicology*, 2005, **214**, 167.
42 Y. Y. Liu, S. Y. Moon, J. T. Hupp and O. K. Farha, *ACS Nano*, 2015, **9**, 12358.
43 V. Kumar and E. V. Anslyn, *Chem. Sci.*, 2013, **4**, 4292.
44 J. Gu, M. Liu, S. Xun, M. He, L. Wu, L. Zhu, X. Wu, W. Zhu and H. Li, *Mol. Catal.*, 2020, **483**, 110709.
45 Y. Cao, Q. Chen, C. Shen and L. He, *Molecules*, 2019, **24**, 2069.
46 C. Wang, Z. Chen, X. Yao, Y. Chao, S. Xun, J. Xiong, L. Fan, W. Zhu and H. Li, *Fuel*, 2018, **230**, 104–112.
47 J. K. Li, C. P. Wei, Y. Y. Wang, M. Zhang, X. R. Lv and C. W. Hu, *Inorg. Chem. Commun.*, 2018, **87**, 5.
48 X. Huang, Y. Cui, J. Zhou, Y. Zhang, G. Shen, Q. Yao, J. Li, Z. Xue and G. Yang, *Chin. Chem. Lett.*, 2022, **33**, 2605–2610.
49 A. Kumar, M. Devi, N. Mamidi, K. E. Gonsalves and C. P. Pradeep, *Chem. – Eur. J.*, 2015, **21**, 18557–18562.

50 Y. Kaya, A. Erçağ, Y. Zorlu, Y. Demir and İ. Gülçin, *JBIC, J. Biol. Inorg. Chem.*, 2022, **27**, 271–281.
51 M. Aureliano and D. C. Crans, *J. Inorg. Biochem.*, 2009, **103**, 536–546.
52 A. Kar and C. P. Pradeep, *Dalton Trans.*, 2020, **49**, 12174–12179.
53 J. Kasperkiewicz, J. A. Kovacich and D. Lichtman, *J. Electron Spectrosc. Relat. Phenom.*, 1983, **32**, 123–132.
54 K. Hakouk, O. Oms, A. Dolbecq, H. El Moll, J. Marrot, M. Evain, F. Molton, C. Duboc, P. Deniard, S. Jobic, P. Mialane and R. Dessapt, *Inorg. Chem.*, 2013, **52**, 555–557.
55 J.-B. Yang, J.-H. Pan, Y.-H. Zhu, J.-L. Wang, H. Mei and Y. Xu, *Inorg. Chem.*, 2022, **61**, 11775–11786.
56 K.-J. Liu, J.-H. Deng, J. Yang, S.-F. Gong, Y.-W. Lin, J.-Y. He, Z. Cao and W.-M. He, *Green Chem.*, 2020, **22**, 433–438.
57 Y. Pan, H. Tian and Z. Zheng, *Inorg. Chem.*, 2024, **63**, 5487–5496.
58 B. Yu, A.-H. Liu, L.-N. He, B. Li, Z.-F. Diao and Y.-N. Li, *Green Chem.*, 2012, **14**, 957–962.
59 Y. Shimizu, Y. Obora and Y. Ishii, *Org. Lett.*, 2010, **12**, 1372–1374.
60 H. Tian, Y. Pan, N. Xu, J. Miao and Z. Zheng, *Inorg. Chem.*, 2023, **62**, 20228–20235.
61 S. Chowdhury, A. Sharma, P. P. Das, P. Rathi and P. F. Siril, *J. Colloid Interface Sci.*, 2024, **665**, 988–998.
62 A. Kar, L. Sharma, A. Kumar, A. Halder and C. P. Pradeep, *Eur. J. Inorg. Chem.*, 2022, **2022**, e202101031.
63 D. Jana, H. K. Kolli, S. Sabnam and S. K. Das, *Chem. Commun.*, 2021, **57**, 9910–9913.
64 S. Kothandan and A. Sheela, *Mini-Rev. Med. Chem.*, 2021, **21**, 1909–1924.
65 J. Li, D. Zhang, Y. Chi and C. Hu, *Polyoxometalates*, 2022, **1**, 9140012.
66 Y. Leng, J. Liu, P. Jiang and J. Wang, *Chem. Eng. J.*, 2014, **239**, 1.
67 B.-B. Lu, J. Yang, Y.-Y. Liu and J.-F. Ma, *Inorg. Chem.*, 2017, **56**, 11710–11720.
68 A. F. Shojaei, M. A. Rezvani and M. H. Loghmani, *Fuel Process. Technol.*, 2014, **118**, 1–6.
69 A. Unnikrishnan and R. B. Sunoj, *Chem. Sci.*, 2019, **10**, 3826–3835.
70 C. Li, N. Mizuno, K. Murata, K. Ishii, T. Suenobu, K. Yamaguchi and K. Suzuki, *Green Chem.*, 2020, **22**(12), 3896–3905.
71 M.-Y. Yu, T.-T. Guo, X.-C. Shi, J. Yang, X. Xu, J.-F. Ma and Z.-T. Yu, *Inorg. Chem.*, 2019, **58**, 11010–11019.
72 N. Tang, Y. Zhang, F. Lin, H. Lü, Z. Jiang and C. Li, *Chem. Commun.*, 2012, **48**, 11647–11649.
73 J.-P. Cao, Y.-S. Xue, N.-F. Li, J.-J. Gong, R.-K. Kang and Y. Xu, *J. Am. Chem. Soc.*, 2019, **141**, 19487–19497.
74 K. Kim, O. G. Tsay, D. A. Atwood and D. G. Churchill, *Chem. Rev.*, 2011, **111**, 5345–5403.
75 B. M. Smith, *Chem. Soc. Rev.*, 2008, **37**, 470–478.
76 D. A. Giannakoudakis, M. Barczak, M. Florent and T. J. Bandosz, *Chem. Eng. J.*, 2019, **362**, 758–766.
77 Y. Hou, H. An, Y. Zhang, T. Hu, W. Yang and S. Chang, *ACS Catal.*, 2018, **8**, 6062.
78 J. K. Li, J. Dong, C. P. Wei, S. Yang, Y. N. Chi, Y. Q. Xu and C. W. Hu, *Inorg. Chem.*, 2017, **56**, 5748.
79 M.-H. Li, S.-L. Lv, M.-H. You and M.-J. Lin, *Cryst. Growth Des.*, 2021, **21**, 4738–4745.
80 B. Picard, I. Chataigner, J. Maddaluno and J. Legros, *Org. Biomol. Chem.*, 2019, **17**, 6528–6537.
81 O. V. Dolomanov, L. J. Bourhis, R. J. Gildea, J. A. K. Howard and H. Puschmann, *J. Appl. Crystallogr.*, 2009, **42**, 339.
82 G. Sheldrick, *Acta Crystallogr., Sect. A:Found. Crystallogr.*, 2008, **64**, 112–122.